

ESTIMATING INDIVIDUAL TREE HEIGHTS AND DBHS FROM VERTICALLY DISPLACED SPHERICAL IMAGE PAIRS

H. WANG , T.R. YANG , J. WALDY , J A KERSHAW, JR.

University of New Brunswick, The Faculty of Forestry and Environmental Management, Fredericton, NB, Canada

ABSTRACT. Individual tree parameters, such as diameter at breast height (DBH) and tree height, are fundamental measurements in forest inventory, and often labour intensive and require significant financial expenditures. Applying digital imaging in forest inventory is an efficient way to decrease the workload. In this study, spherical images taken using a novel commercial 360° camera (Ricoh Theta S) and stereographic geometry were applied to obtain these parameters directly without stitching multiple images from common cameras. This technology was validated in both a sparse urban forest (pairwise comparison) and denser real forest (distributional comparison) in Atlantic Canada. The DBH ($r^2 > 0.76$) and height (Dmax < 0.25 , K-S test) showed high correspondence with field measures. The spherical camera represents a low-cost option to terrestrial laser scanning and has potential to produce more accurate forest-level estimates with quicker field and office processing time than current under-canopy remote sensing technologies.

Keywords: panorama images; digital camera; forest inventory; remote sensing; horizontal point sampling

1 INTRODUCTION

Forests are the dominant terrestrial ecosystems and account for over three quarters of gross primary productivity and plant biomass on the Earth (Pan et al., 2013). They provide many ecosystem services including watershed protection, soil structure maintenance, and global carbon storage. Individual tree stem attributes, such as diameters, heights and spatial locations, are critical measurements in most forest inventories (Kershaw et al., 2016), and are the fundamental variables used in allometric equations to estimate biomass, volume, and carbon (Blake et al., 1991; Hayashi et al., 2015; Lambert et al., 2005; Smith and Brand, 1983; Xing et al., 2005; Zianis et al., 2005). How to measure these parameters across extensive forest areas with high efficiency and low costs is a continuing challenge for all forest inventory specialists (Gadow et al., 2009; Husch, 1980).

For under canopy tree measurements, traditional tools such as diameter tapes and clinometers are widely used. These basic tools have been modified and digitized to make field data collection more efficient, including optical callipers, rangefinder dendrometers, and optical forks (Clark et al., 2000a). Although several of these instruments have high accuracy and precision, the high costs and the continued focus on individual trees limit wide-

spread use. Hence, many instruments have disappeared from the market (Clark et al., 2000a; Perng et al., 2018; Shimizu et al., 2014). Laser and sonic instruments for measuring tree heights have had greater success than digital instruments for diameter measurement (Clark et al., 2000a). The success of these instruments over similar ones for DBH measurement is probably due to the difficulty and time-consuming nature of height measurement using traditional tools. More repeatable measurements and reduced field time has contributed to these instruments being widely adopted in forest inventory operations.

Photogrammetry has a long history of use in forestry. Reineke (1940) was among the first to develop the idea of using terrestrial photos in forest inventory. However, use of photos requires establishing scale. Field measured distances were commonly used in early studies (Clark et al., 2000a,b). Another popular method to establish scale was the use of reference targets with known lengths or sizes (poles, tags, or laser facula). These methods have been widely applied in photogrammetry studies (Celes et al., 2019; Dean, 2003; Pengele et al., 2013; Shimizu et al., 2014; Varjo et al., 2006). Multiple photos with known shifts in position also can be used to establish scale stereographically (Clark et al., 1998).

Many studies focus only on single tree images and individual tree measurements. However, for inventory efficiency, methods to extract estimates for multiple trees without the need to shift the camera for each tree of interest are required (Perng et al., 2018; Stewart, 2004). DeCourt (1956) demonstrated how printed photos and manual processing could be used to estimate basal area per ha using angle count sampling methods (Bitterlich, 1984). With the advent of affordable digital cameras, Stewart (2004) revived this idea and took a series of 8 photographs to represent the plot, while Fastie (2010) used ultra-high resolution panoramas stitched from 504 photos to estimate stand basal area. In both studies, the angle gauge was expressed in terms of pixel widths and trees with pixel widths greater than the angle gauge pixel width were counted as "in". Dick et al. (2010) used a single row of 24 horizontal photos to map tree locations from stitched panoramas.

Lu et al. (2019) recently expanded this idea to measure tree diameters at different heights. However, for parameters other than stand basal area based on angle count sampling, all of these studies required scale tags (Dick et al., 2010; Lu et al., 2019) on each tree or measured field distances and slopes (Lu et al., 2019). Measuring or tagging individual trees is time consuming and costly, and, other than providing a permanent record of field conditions, the photos have no benefit for improving field inventory efficiency. In addition, errors resulting from the stitching of several digital image cannot be avoided (Dick et al., 2010; Fastie, 2010; Lu et al., 2019; Perng et al., 2018).

Using wide-angle hemispherical lenses has potential to eliminate errors caused by stitching images and could potentially simplify calculations. Paired fisheye cameras have been used to obtain stem diameter, basal area, location mapping and volume without dependence on field measurements (Rodríguez-García et al., 2014; Sánchez-González et al., 2016; Wang et al., 2020). Berveglieri et al. (2017) developed an automated algorithm by matching hemispherical images at different heights to estimate stem diameters. More recently, the development of affordable 360° spherical cameras offer new opportunities for obtaining optical tree measurements (Perng et al., 2018). Spherical cameras, like the Ricoh Theta S (Ricoh Imaging Company, LTD., 2016), offer an inexpensive option for obtaining spherical inventory images directly. The compact size of a spherical camera makes it an easy-to-use tool in the forest and can be moved through the canopy using a height pole to obtain structural estimates more easily than traditional fisheye cameras and other digital cameras.

Structure from motion (SfM) technology enables three-dimensional (3D) reconstruction from image series without actual measurements (Fang and Strimbu, 2017;

Sanvely et al., 2008). This technique has been applied to 3D reconstruction of individual stems (Larsen, 2006a,b; Miller et al., 2015; Mokroš et al., 2018; Surový et al., 2016), and to stand level forest point cloud development (Forsman et al., 2016; Liang et al., 2014, 2015; Liu et al., 2018). The mapping accuracy from SfM is similar to TLS (Liang et al., 2014). However, SfM technologies often require walking through sample plots and obtaining a large number of photos (Berveglieri et al., 2017; Liu et al., 2018). Mulverhill et al. (2019) integrated SfM with a spherical camera to generate 3D plot point clouds and significantly decreased the number of photos required for accurate point cloud rendering. The results showed high correspondence with field measured data (Mulverhill et al., 2019). Although the procedures are mostly automatic, the point cloud generation and analyses requires a high performance computer and complex algorithms (Belton et al., 2013; Liang et al., 2015; Mulverhill et al., 2019). It also might be questioned as to the need to generate a 3D point cloud and then do measurements, when those basic measurements often can be done directly on the images. Based on this, we identified a need for a simplified system for obtaining spherical photos in stereo.

The goal of this study was to develop an approach to obtain such spherical image pairs and apply stereoscopic geometry to estimate diameter and height of individual trees directly without any field measurement dependency. The specific objectives were to: 1) derive the geometry for two vertically displaced spherical image pairs to estimate desired tree attributes; 2) validate the technique in a sparse urban forest setting; and 3) perform a preliminary field assessment in a real forest situation.

2 METHODS

2.1 Study sites

Urban Site – The University of New Brunswick campus located in Fredericton, New Brunswick, Canada (Fig. 1) was used for validating the approach in an open situation where visibility was not a substantial issue. Two ditial sampling points were selected for this phase of the study. The criteria for sample point selection included: 1) Open forest conditions with a moderate number of trees (7-12 trees) with each tree's tip and base clearly visible; 2) Individual trees have varying distances from the image sampling points; and 3) Individual trees have varying diameters and heights.

Forest Site – An early spacing trial located on the western side of Newfoundland (NL) Island, near Roddickton, Newfoundland and Labrador, Canada (Fig. 1) was used for testing the approach in a real forest condition. The spacing trial, with different densities and

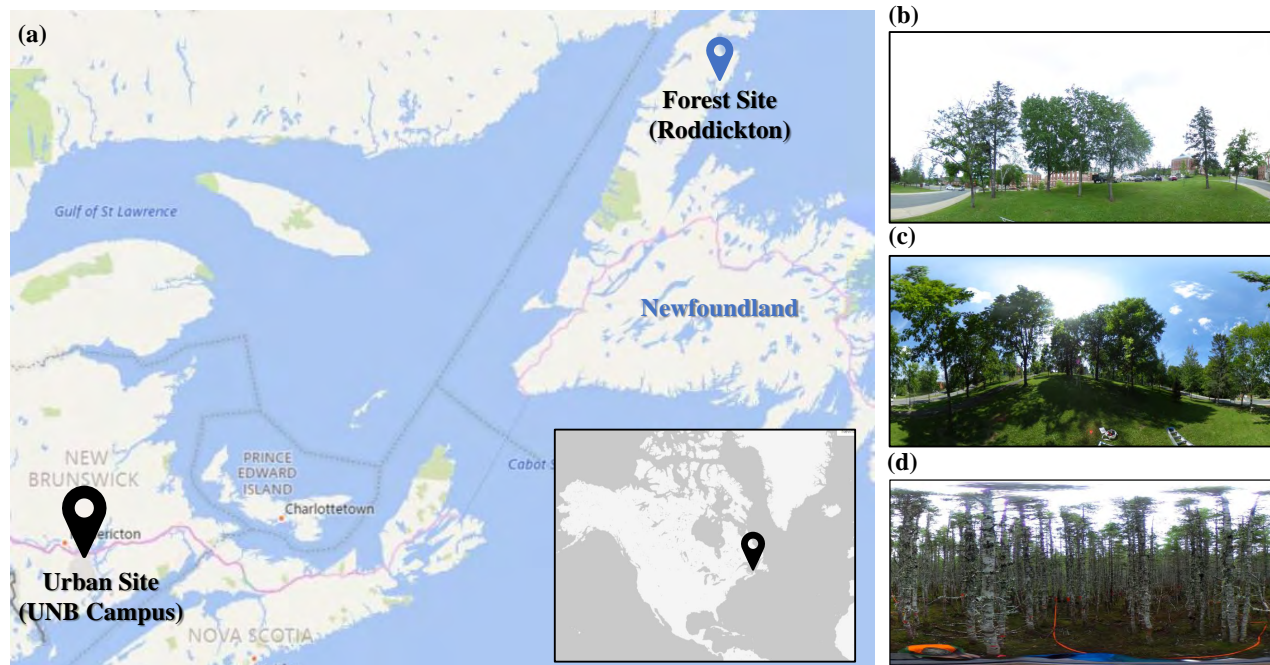


Figure 1: The study sites locations (and associated topography) used in this study. (a) a map of Atlantic Canada showing the urban and forest site locations, (b) and (c) are photos of the two urban sites, and (d) is a cylindrical projection of one of the forest sites in Roddickton, NL.

different resulting tree sizes, was an ideal field setting for this test. The site was dominated by balsam fir (*Abies balsamea*) with minor components of black spruce (*Picea mariana*) and other boreal species. The trial was established in the early 1980's (Donnelly et al., 1986). Five spacing treatments were applied: Control (no spacing), 1.2m, 1.8m, 2.4m, and 3.0m average spacing. Plot radii varied by spacing treatment (Control (5.2m); 1.2m (7.2m); 1.8m (10.4m); 2.4m (15.0m); 3.0m (18.0m)) with the aim of having about 100 trees per plot at the time of treatment establishment (Donnelly et al., 1986). At the time of the initial treatments, the site was a naturally regenerating even-aged stand. The spacing treatments produced plots that were single strata with relatively uniform stand structures within spacing treatments.

2.2 Data collection

2.2.1 Digital image pairs

A Ricoh Theta S (Ricoh Imaging Company, LTD., 2016) spherical camera was used to capture spherical images. Two single spherical images were captured at 1.6m and 2.6m above ground (camera was mounted on a height pole stabilized by a tripod (Fig. 2.a) for each digital sampling point in both study sites. A bubble level attached to the tripod was used to ensure relative level of two images captured at different heights.

On the Urban Site, two independent single digital sampling points were located strategically among the trees of interest (Fig. 2.b) to ensure visibility and a variety of camera to tree distances. On the forest site, three digital sample points per replicate plot were used (Fig. 2.b). Multiple digital sample points were used to minimize tree occlusion and facilitate measurement of as many plot trees as possible. Digital sample points were located at half the plot radii at azimuths of 0° , 120° , and 240° . On the forest site, three digital sample points per replicate plot were used (Fig. 2.b). Multiple digital sample points were used to minimize tree occlusion and facilitate measurement of as many plot trees as possible. Digital sample points were located at half the plot radii at azimuths of 0° , 120° , and 240° .

Although the spherical camera recorded 360° spherical images, the images were stored like a common digital camera pixel matrix using cylindrical equidistant projections generated automatically by the Ricoh Theta S onboard software. The resolution of the projected cylindrical images was 5367 pixels in width and 2688 pixels in height.

2.2.2 Urban site data

The urban site was used to validate the algorithm and method. The sampling points were located where all trees' bases and tops were clearly visible. For each se-

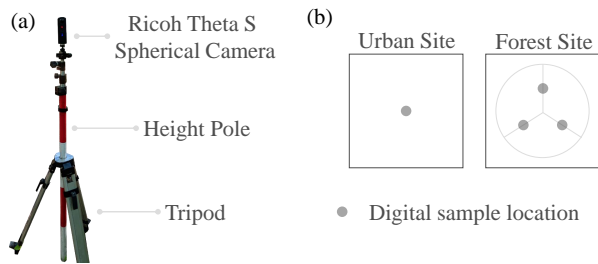


Figure 2: Digital data collection methods. (a) tripod, height pole and spherical camera set up for spherical image acquisition at two different heights (1.6m and 2.6m). (b) Digital sample location designs for the urban area validation study and the real forest application. For the urban site, only one location was set. For the forest site, three locations were established at the midpoint of plot radius along azimuths of 0° , 120° , and 240° .

lected tree, flagging tape was wrapped around the tree circumference at breast height (1.3m) to facilitate visibility and a numbered target placed on each tree to facilitate matching field and image measurements. The radial distance from sampling points to each tree (FieldR) was measured with a TruPulse laser hypsometer. Generally, the cross-sections of tree trunks are not perfect circles and are often elliptical (Kershaw et al., 2016). The diameter projected onto an image may vary substantially depending on projection azimuth and tree eccentricity, therefore, the DBH of each tree was measured using calipers along the tree axis perpendicular to the projection azimuth (ProjectedDBH) and measured with a diameter tape (FieldDBH). Tree height (HT) was measured in the field from 2 different perspectives using a TruPulse laser hypsometer: 1) the height measured at the image sampling point (ProjectedHT); and 2) from a convenient and reasonable location from which to clearly see tree tip and base (FieldHT).

2.2.3 Forest site data

As with the urban site data, DBH (nearest 0.1cm) and HT (nearest 0.1m) of each individual tree in one replicate from the Roddickton spacing trial were measured using a diameter tape and laser hypsometer. However, the spherical images were acquired for a different study other than individual tree measurement, and field trees were not individually identified and tagged in the field such that they could not be easily aligned on the spherical images. Therefore, comparisons between field measurements and spherical measurements were limited to plot level distributions rather than individual tree level pairs.

2.2.4 Image processing geometry

The general workflow included: 1) determining the projection algorithm to exchange pixel coordinates in the cylindrical images to latitude and longitude in spherical coordinates; 2) marking the bases and tips of individual trees on the cylindrical images, applying spherical geometry to estimate the distances from digital sampling points, slope deviations and tree heights; and 3) determining the vertical pixel coordinate (y) for breast height (1.3m) in the cylindrical images, marking the left and right tree trunk edges (horizontal angles) at 1.3m, determining the intersection angles to camera center, and estimating DBHs using spherical geometry.

1) Cylindrical images were converted to spherical images using the methods proposed by Aghayari et al. (2017). For a given point in cylindrical coordinates (x_i, y_i), the transformed spherical angles (longitude and latitude) were given by:

$$\begin{aligned} lon_i &= (X - x_i) \cdot \frac{2\pi}{X} \\ lat_i &= (y_i - \frac{Y}{2}) \cdot \frac{\pi}{2Y} \end{aligned} \quad (1)$$

where X was the cylindrical image width in pixels (5367 pixels for the images used in this study); Y was the cylindrical image height in pixels (2688 pixels for the images used in this study); x_i was the horizontal pixel coordinate; and y_i was the vertical pixel coordinate. Latitude angles (lat_i) ranged from $-\frac{\pi}{2}$ (-90°) to $\frac{\pi}{2}$ (90°) while Longitude angles (lon_i) ranged from 0 (0°) to 2π (360°).

2) As shown in Figure 3.a, after marking the tree tip and base (the bole at ground level) in both cylindrical images manually, 4 latitudinal angles were calculated from Equation 1. The elevation difference between sampling point and tree base (Δh) was:

$$\Delta h = \frac{Z_2 \cdot \tan(\beta_1) - Z_1 \cdot \tan(\beta_2)}{\tan(\beta_1) - \tan(\beta_2)} \quad (2)$$

and radial distance (R) was then obtained using:

$$\begin{aligned} R_1 &= \frac{Z_1 - \Delta h}{\tan(\beta_1)} \\ R_2 &= \frac{Z_2 - \Delta h}{\tan(\beta_2)} \end{aligned} \quad (3)$$

where $Z_1 = 1.6\text{m}$ and $Z_2 = 2.6\text{m}$ (the camera heights in this study). R was estimated as the average of R_1 and R_2 .

From Figure 3.b, tree HT was derived using:

$$\begin{aligned} HT_1 &= Z_1 - \Delta h + R \cdot \tan(\tau_1) \\ HT_2 &= Z_2 - \Delta h + R \cdot \tan(\tau_2) \end{aligned} \quad (4)$$

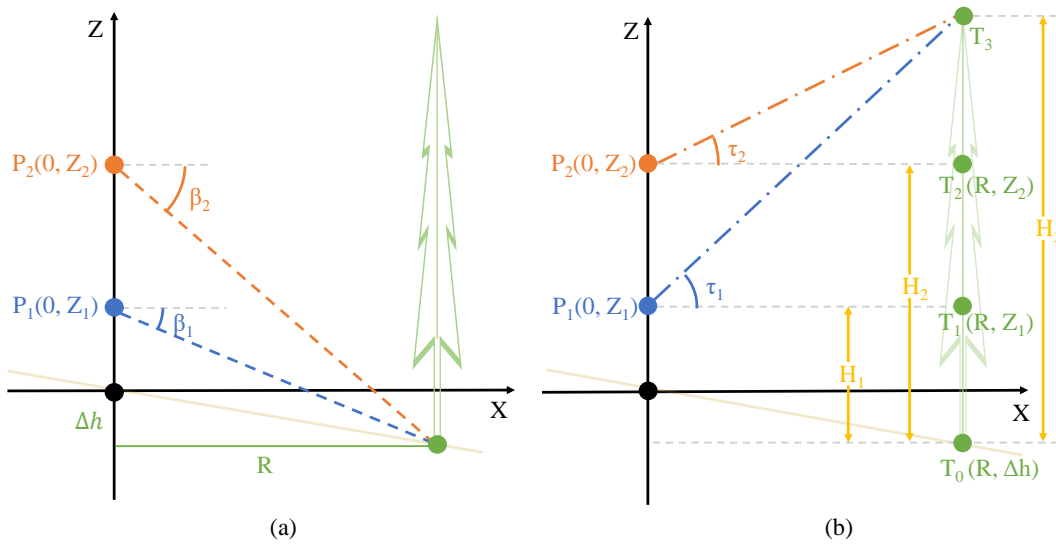


Figure 3: The distance, slope deviation, and tree height calculation from the vertical projection of the spherical geometry: (a) derived distance (R) and slope deviation (Δh) caused by terrain variation derived from the key points for tree bases. (b) height calculation based on several key points for tree tips and along on the bole.

Tree HT, as defined by these relationships is the perpendicular distance from ground to tree tip, as is typically measured in most forest inventories (Kershaw et al., 2016), rather than stem length. HT was estimated as the average of HT_1 and HT_2 .

3) For DBH estimation, it was necessary to locate the 1.3m height on each image. The angle from horizontal to 1.3m was estimated for each image (Fig. 4.a) using:

$$\begin{aligned}\gamma_1 &= \tan^{-1} \left(\frac{1.3m - (Z_1 - \Delta h)}{R} \right) \\ \gamma_2 &= \tan^{-1} \left(\frac{1.3m - (Z_2 - \Delta h)}{R} \right)\end{aligned}\quad (5)$$

As with the other parameters, γ was estimated as the average between γ_1 and γ_2 . DBH was then estimated from the tree projection angles for each tree on each image (Fig. 4.b). Tree projection angles (ω) were estimated by marking the left (B_l) and right (B_r) tree edges:

$$\begin{aligned}\omega_1 &= 360^\circ \cdot \left(\frac{x_{r,1} - x_{l,1}}{X} \right) \\ \omega_2 &= 360^\circ \cdot \left(\frac{x_{r,2} - x_{l,2}}{X} \right)\end{aligned}\quad (6)$$

Then distance from camera to the tree center, as shown in Figure 4.c, was the slope distance (L) shown in Figure 4.b:

$$L_i = \frac{R + \frac{DBH_i}{2}}{\cos(\gamma_i)} \quad (7)$$

In Figure 4.c, DBH also was represented by the spherical geometry based on the basal area factor derivation (Kershaw et al., 2016):

$$DBH_i = 200 \cdot L_i \cdot \sin(\omega_i) \quad (8)$$

Solving Equation 7 and Equation 8, DBH was equal to:

$$DBH_i = \frac{200 \cdot R \cdot \sin(\frac{\omega_i}{2})}{\cos(\gamma_i) - \sin(\frac{\omega_i}{2})} \quad (9)$$

As with R and HT, DBH was estimated as the average from the two images: $DBH = (DBH_1 + DBH_2) / 2$.

To facilitate extraction of the required image measurements, a graphical interface (Fig. 5) was developed in Python 3.6 (Guido, 2018) to mark key points for trees and for calculating the required parameters as illustrated in Figs. 3 and 4. The interface can be downloaded from <https://github.com/Howcanoewang/Spherical2TreeAttributes/releases>.

2.3 Data analysis

2.3.1 Urban data analysis

To validate the accuracy of our approach, a pairwise linear regression was fitted to the field and image measurements for R , DBH, and HT:

$$Field = b_0 + b_1 \cdot Photo \quad (10)$$

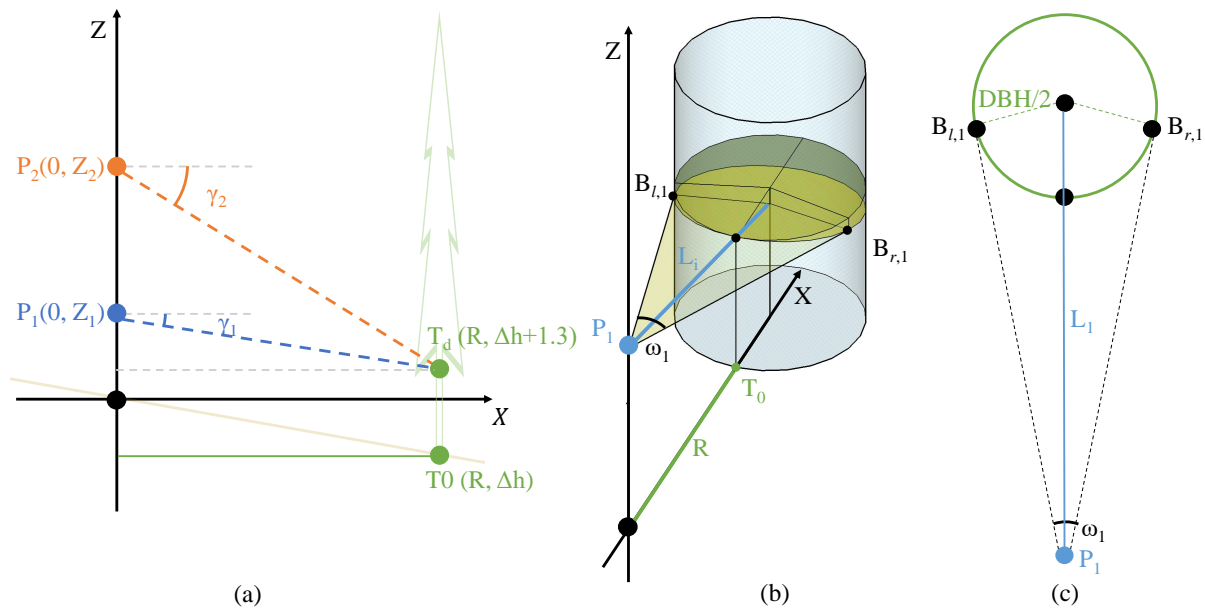


Figure 4: DBH calculation using spherical geometry. (a) calculation of the 1.3m height on the images. (b) DBH boundary marking and distance to tree center derived from stereo coordinates (based on the 1.6m height image as an example); and (c) geometrically derived DBH.

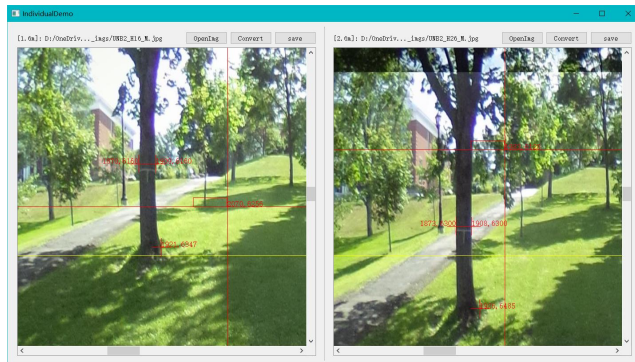


Figure 5: The graphical user interface used to mark key point coordinates for individual trees for parameter calculation. The images shown in this figure are from urban plot B with a steep slope. The yellow line indicates the image horizon (image equator) of spherical image.

If image estimates were identical to field estimates, then $b_0=0$ and $b_1=1$. The resulting parameter estimates were tested for these values using t-tests and Bonferroni-adjusted α levels (Zar, 2009).

The agreement between field and image measurements were also evaluated by root mean square error (rMSE) and root mean square error expressed as a percentage of mean (%rMSE):

$$rMSE = \sqrt{\frac{\sum_i^n (Image_i - Field_i)^2}{n}} \quad (11)$$

$$\%rMSE = 100 \cdot \frac{rMSE}{Field_{mean}} \quad (12)$$

2.3.2 Forest data analysis

The images from the Roddickton spacing trials were originally taken for area-based estimation, not individual tree measurement, so the trees were not tagged. Instead of using pairwise statistical tests, we focused on distributional statistics at the plot level to compare DBH and HT estimates. The two-sample Kolmogorov-Smirnov (K-S) test (Hodges, 1958) which tests whether two samples were drawn from the same continuous distribution, was used here. Our null hypothesis was that the field measured samples and image measured samples were identically distributed. The alternative hypothesis was that they were not identically distributed. We assume that equal distributions convey a level of confidence that our technique was measuring DBH and HT correctly. This assumption ignores potential bias in tree visibility in the images and repeat observation of the same trees across the three digital sampling points.

3 RESULTS

3.1 Urban forest validation

Figure 6.a shows the relationships between field measured distance (FieldR) and image estimated distance (ImageR). While the ImageR was slightly overestimated compared with FieldR, the simple linear regression (Tab. 1) showed no significant differences ($p > 0.05$) from the hypothesized parameter estimates and had a high r^2 and low root mean square error (rMSE). ImageHT was not significantly different ($p > 0.05$) from ProjectedHT (Fig. 6.b), which is the field measured height at the digital sample points; however, ImageHT was significantly different ($p < 0.05$) from FieldHT, which is the field measured height from a point where tree tips can be clearly observed. As FieldHT increased, there was a trend of increasing overestimation associated with ImageHT (Fig. 6.c). The significance of these trends was confirmed by the linear regressions (Tab. 1.). For DBH estimation (Fig. 6.d-e), the b_{0s} and b_{1s} were not significantly different from 0 and 1, respectively, ($p > 0.05$) for both ProjectedDBH (measured by calipers along the tree axis perpendicular to the projection azimuth) and FieldDBH (measured by diameter tape). The high r^2 s (0.96) and low rMSEs (around 2.4) confirmed strong linear relationships between image measured DBHs and field measured DBHs. The percentage root mean square errors (%rMSE) without unit concern in Table 1 demonstrated that the both DBH (FieldDBH and ProjectedDBH) was estimated more consistently than the FieldHT, but similar to ProjectedHT.

3.2 Field forest test

The distributional comparisons between field measured attributes and image estimated attributes for the

Roddickton, NL spacing trial are shown in Figure 6 and the K-S test results are given in Table 2. With the exception of the 1.2m spacing treatment, the number of measurable trees on the images were lower than the number of trees measured on the actual field plots (Tab. 2), despite having 3 digital sample points per plot.

The results obtained in the forest situation were different from what were observed in the urban setting. With the exception of the Control spacing treatment (S00), all image HT distributions were not significantly different ($p > 0.05$) from field distributions (Fig. 7.f-j and Tab. 2). On the other hand, only the 3.0m spacing (S30) produced DBH distributions that were not significantly different from field distributions (Fig. 7.e and Tab. 2). These results are the opposite of what was observed in the Urban situation where DBH was estimated consistently more accurately than HT (Fig. 6.d-e and Tab. 1).

4 DISCUSSION

The goal of this study was to examine the potential of using spherical images to estimate individual tree diameter and height. This method was applied in an open urban setting and in a real forest situation. Our results observed a good correspondence with field measured data in the urban area, while the real forest results were mixed.

Our urban site validation showed that correspondence between image measured and field measured DBHs was high for both ProjectedDBH (measured by caliper at image view angle) and for FieldDBH (measured with diameter tape) (Fig. 6.). However, for the real forest test, the results were not as positive. Distributions of image derived DBHs were consistently larger than distributions of field measured DBHs (Fig. 7.). For height estimation, the urban forest study showed a high corre-

Table 1: Simple linear regression results between photo estimates and field measurements. The linear model is $Y = b_0 + b_1 * X$, if Photo measured (X) is the same as Field measured (Y), then $b_0 = 0$ and $b_1 = 1$. In table header, YRange is the range of Y values = (min, max); Param. = Parameter; Est. = Estimate; SE = Standard Error; rMSE = root Mean Square Error; %rMSE = root mean square error expressed as a percentage of mean.

X	Y	YRange	Param.	Est.	SE	p-value	r^2	rMSE	%rMSE
ImageR	FieldR	(2.7, 27.7)	b0	-0.180	0.542	0.743	0.974	0.153	7.111
			b1	1.058	0.039	0.153			
ImageHT	ProjectedHT	(9.4, 25.6)	b0	0.653	0.743	0.390	0.949	0.971	6.794
			b1	0.990	0.052	0.851			
ImageHT	FieldHT	(9.4, 23.1)	b0	3.954	1.245	0.005	0.762	1.627	12.074
			b1	0.692	0.087	0.002			
ImageDBH	ProjectedDBH	(12.3, 69.6)	b0	-1.246	1.546	0.430	0.966	2.398	7.167
			b1	1.039	0.044	0.378			
ImageDBH	FieldDBH	(12.8, 69.6)	b0	0.116	1.578	0.942	0.962	2.448	7.321
			b1	0.999	0.044	0.963			

Table 2: Summary of KS-Tests for real forest validation. Plot radii varied by spacing treatment (Control (S00, 5.2m); 1.2m (S12, 7.2m); 1.8m (S18, 10.4m); 2.4m (S24, 15.0m); 3.0m (S30, 18.0m)).

Plot	Field Tree #	Image Tree #	Factor	KS Value	p-value
S00	94	63	DBH	0.4262	<0.001
			HT	0.2518	0.0134
S12	56	92	DBH	0.3602	<0.001
			HT	0.2096	0.079
S18	103	60	DBH	0.2589	0.0097
			HT	0.1126	0.6697
S24	137	96	DBH	0.2600	<0.001
			HT	0.1393	0.1982
S30	122	59	DBH	0.1555	0.2573
			HT	0.1188	0.5774

spondence with ProjectedHTs measured from the digital sampling point; however, correspondence was not as high with heights measured from locations where tree tips were clearly visible (FieldHT). However, surprisingly, in the forest situation, image measured heights (ImageHT) were distributed similarly (based on K-S test Dmax values) to field measured heights (FieldHT) for all spacings except S00 (the control plots).

There are several possible explanations for the reversed results observed between the two study areas. First, the urban trees were substantially larger (bigger DBHs and taller heights) than the forest trees. The urban tree HTs ranged from 10m to 25m (Fig. 6.b), and the urban DBHs ranged from 15cm to 70cm (Fig. 6.d), while, the forest trees had a DBH range from 5cm to 25cm with large variation within and between the different spacing treatments (Fig. 7.a-e). Only the 3.0m spacing treatment had low variability within treatment, and this was the treatment that had DBH distributions that were not significantly different ($p > 0.05$) from the field DBH distributions. In contrast to the generally higher variability in DBHs, the forest trees had much lower HT variability within and between the spacing treatments with most field and image-estimated HTs below 15m (Fig. 7.f-j).

Tree density probably played an important role for the differing results observed between the urban and forest study sites. In the urban setting, the trees were well spaced and the boles clearly distinguishable against a background of grass (visibility was further enhanced by the use of flagging tape). In the forested situation, especially for plots with narrower spacings, the tree trunks often overlapped in the background making it very difficult to clearly distinguish the tree edges. The smaller trees were most likely easier to be missed when marking trees for measurement and single pixel width errors had greater impacts. If the trunk edges were not clearly distinguishable, those trees were not marked on the im-

ages. Given that we had three digital sampling points per forest plot, larger trees were probably more visible across multiple images as well, further contributing to the bias toward larger trees. For example, consider S00 and S12 field distributions which showed an abundance of very small trees (Fig. 7.a-b) - these two plots had the worst performance for DBH estimation and had the largest distributional differences in the upper DBH range (Fig. 7.a-b). Because we did not attempt to eliminate repeated measures of trees across the three digital sampling points, this probably contributed significantly to the overestimation problem observed in this study. Furthermore, the problem with hidden trees, which exists in all panoramic images (Dick et al., 2010) and affects smaller trees more frequently, was an additional source of bias in this study.

The uniformity in the field height distributions (Fig. 7.) negated any visibility bias for the image height distributions. In addition, the shorter conifer trees in the forested situation, with their cone-shaped crowns, made it easier to identify the real tree tip. As Kershaw et al. (2016, p. 117) pointed out, there is a tendency to overestimate the height of large, flat-crowned trees using the tangent method.

The irregularity in tree cross-sectional shape did not appear to be a problem in this study, at least in the Urban setting (Fig. 6.). Stem irregularities can cause errors in image derived DBH estimates (Perng et al., 2018). Several studies have addressed this issue by either taking photos at different angles around the stem, or constructing 3D models (Larsen, 2006a) or even generating 3D point clouds to assess stem geometric structure (Liang et al., 2014; Mokroš et al., 2018; Ringdahl et al., 2013; Surový et al., 2016). Though these methods produce small errors (2.2 ± 3.0 cm; Ringdahl et al. (2013)) and low rMSEs (2.39cm for Liang et al. (2014), 1.87cm for Surový et al. (2016), and 1.27cm for Mokroš

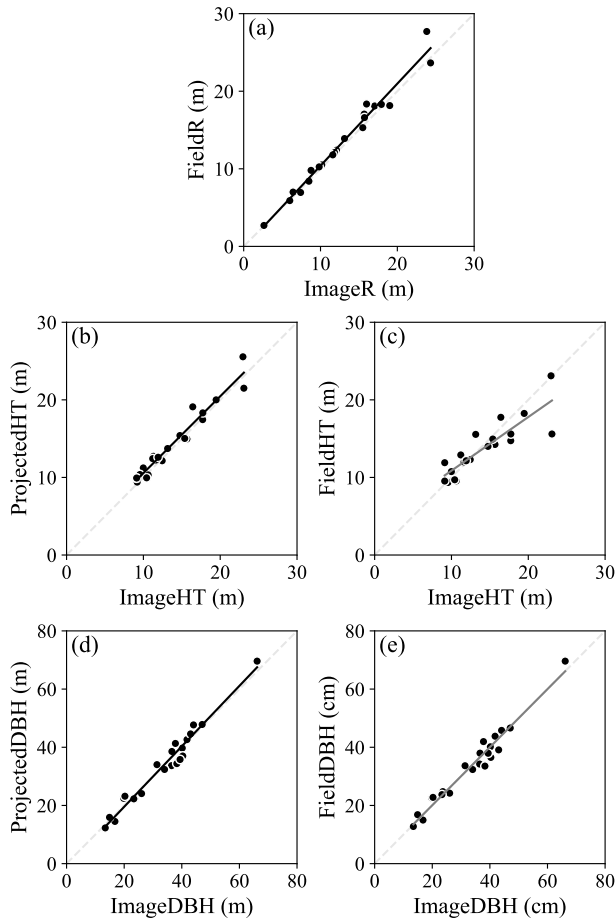


Figure 6: Comparisons between field measurements and image estimates: (a) radial distance (R); (b) digital image height (ImageHT) compared to field height measured HT at the digital sampling points (ProjectedHT); (c) digital image height (ImageHT) compared to field height measured from locations where tree tips are clearly visible (FieldHT); (d) digital image DBH (ImageDBH) compared to projected DBH measured by calipers (ProjectedDBH); and (e) digital image DBH (ImageDBH) compared to DBH measured by diameter tape (FieldDBH).

et al. (2018)), the computation requirements limit their wide-scale application in forest inventories. Our results show, if accounting for optical fork effects (Grosenbaugh, 1963), the errors can be decreased to acceptable levels. In our case, errors were 2.4 ± 1.6 cm. Similarly, Celes et al. (2019) reported an uncertainty of approximately ± 1 cm and Lu et al. (2019) had errors within ± 6 cm with the assistance of field reference targets, while Perng et al. (2018), using similar geometry had a rMSE of 13.19cm.

Decreasing spatial grain with distance is a problem associated with all remote sensing techniques (including LiDAR). Remote sensing is driven by reflection point

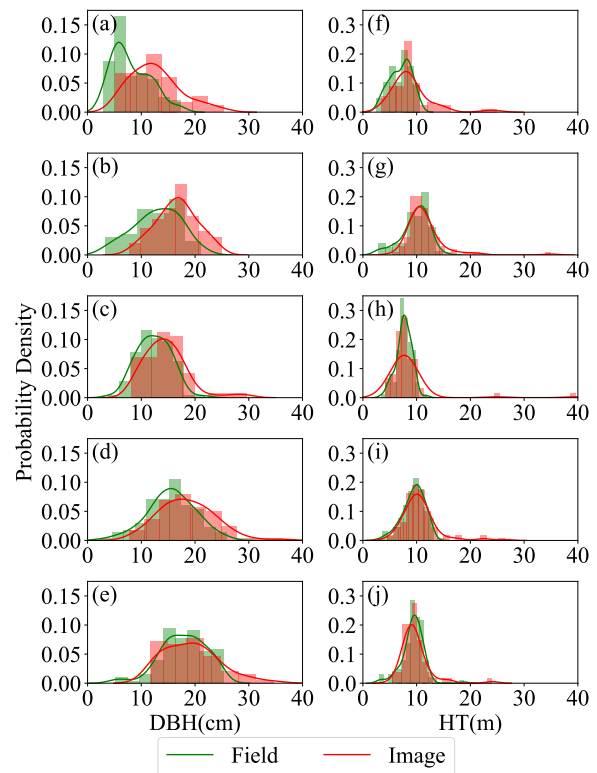


Figure 7: Field measured distributions versus image estimated distributions for DBH and HT by spacing treatment: (a) and (f) Control; (b) and (g) 1.2m Spacing; (c) and (h) 1.8m Spacing; (d) and (i) 2.4m spacing; and (e) and (j) 3.0m Spacing.

values that are averaged over the photon footprint. One point (or pixel) represents an increasing area with increasing distance from digital sampling point. The effects of distance from digital cameras (Dick, 2012; Wang, 2017) and spherical cameras (Wang, 2019; Wang et al., 2020) has been well analyzed. Decreasing accuracy with increasing distance is a limitation of any light-based sensor (Clark et al., 2000a). This issue is exacerbated if the objects of interest are smaller (Reu et al., 2014).

The primary advantage of a spherical camera over a common camera is that we obtain the whole 360° plot in a single image from a single shutter trigger. The image is derived from two fixed fisheye lenses and stitched using the camera's onboard software. Obtaining the whole plot in one image saves a lot of time acquiring images, stitching them together and analyzing images. In order to take a 360° plot using images from a common camera, a heavier tripod with a stabilized rotary table is required to be transported in the forest. At least 15 images are needed to ensure enough overlap between images (Dick, 2012) which requires more field time and office time stitching the photos together. If heights are re-

quired then multiple rows of images must be acquired by tilting the camera at increasing angles, increasing field time, stitching time and analysis time; however, very high resolution images are produced (Fastie, 2010). The trade-offs between field time and increased image resolution versus accuracy of resulting image measurements needs more evaluation. Based on a preliminary study using a common digital camera to measure DBH (Wang, 2017), the higher resolution images showed improved accuracy (42% of trees within $\pm 0.5\text{cm}$ and 25% within $\pm 0.5\text{cm}$ to 1.0cm), while the accuracy for this study was 2.4cm (based on rMSE, Table 1),

The advantages of a spherical camera over a laser scanner include both the instrument costs and data acquisition time. For spherical images, field time is around 5-10 minutes per plot, and around 4-5 minutes for processing each image pair (about 1-2 mins to align the paired images, and about 3 mins to click the key points for all trees and processing the measurements. Adapting an hierarchical subsampling scheme could significantly reduce processing time without substantially reducing accuracy (Dai, In review). TLS technology continues to improve and both fixed-base and mobile scanners are available, Using a FARO (FARO Technologies, Inc. Florida, U.S.) X330 Scanner, three in-plot scans required about 45 minutes, and 2-3 hours for software stitching the three scans together. Point cloud processing can take up to 5 hours depending upon which tree measures are required and what algorithms used without any real gains in accuracy over what we obtained here (Gollob et al., 2019). As a benchmark comparison, field measurement of plot trees can range from about 20 minutes to 2-3 hours depending on plot size, plot type, and the different tree measurements required.

The manual clicking of key points, as implemented in this study, introduces the possibility of inter-observer errors and biases. Based on our previous application of spherical images implementing angle count sampling on spherical images (Wang, 2019; Wang et al., 2020), inter-observed differences were affected by the complexity of spherical images. For images obtained in sparse forests with bigger trees and clear trunk boundaries, the consistency was higher than dense forest images. This is likely to be an issue with the clicking for DBH and HT measurements developed here. Automatic detection algorithms may help decrease the subjectivity, but, as figure 1.d shows, this is a complicated common computer vision task requiring thousands of annotated training images for deep learning based algorithms to be effective, and is far beyond the scope of this study.

One of the biggest limitations for applying spherical images to whole plot measurement is tree visibility, not only for small trees far away from plot center with very narrow view angles, but also for trees occluded by larger

trees near plot center. Non-detection bias is a significant concern with any remote sensing technology, Multiple scans from different locations within plots can reduce occlusion (Ritter et al., 2013). Instead of basing area-based estimates on fixed area sampling methods, angle count sampling (Wang et al., 2020) is a powerful sampling technique that could eliminate or minimize non-detection biases. By controlling the basal area factor, the visibility issue can be controlled (Dick, 2012; Wang et al., 2020). Multiple digital sampling points, as implemented in this study, can reduce the number of hidden trees, though this introduces the unavoidable duplicate marking of some trees with potential bias toward larger trees (Figure 7).

The projection distortion produced by the cylindrical projection of the spherical images is another factor limiting the current method. Trees very close to camera location become very distorted making the tree tips very difficult to determine. This issue limits the applicability of subsampling schemes like big-BAF sampling (Iles, 2012) because this method inherently selects trees that are closer to the digital sampling point. Finally, we only tested and validated our approach in a conifer dominant forest with tree heights around 15m. It may difficult to apply in forests with taller trees or composed of dense broad leaved species. Conditions which are likely to result in increased distortion issues.

One of the key next steps is to replicate the measurement protocols used in the urban setting in a forested situation where field and image measurements are matched. This will help eliminate some of the uncertainty we obtained in our forested test. Time-motion studies comparing field measurement times with image measurement times would also provide additional insight into gains in measurement efficiency and accuracy associated with this technique.

5 CONCLUSION

Though using camera photos in forest inventory has a long history and earlier studies have tried diverse methods to estimate typical forest attributes, the use of vertical paired spherical cameras (Ricoh Theta S) and stereoscopic geometry to calculate attributes directly has not been explored. Our results show this novel technology can achieve good correspondence with field measured tree metrics in simple urban conditions (sparse and big trees). For complex and dense forest conditions, it achieved moderate correspondence, as measured by the K-S two-sample distribution test for DBH and HT estimation. The spherical camera represents a low cost alternative to terrestrial laser scanning for the estimation of DBHs, heights, and possibly stem form. Field work is greatly reduced and data processing is much sim-

pler. Integration into a hierarchical subsampling design is likely to be the most efficient use of the methods developed in this study

ACKNOWLEDGEMENTS

The authors declared no Conflict of interest. And this work was partly supported by the National Science and Engineering Research Council of Canada, Discovery Grants program, the Province of Newfoundland and Labrador Centre for Forest Science and Innovation Contribution Agreement, and the New Brunswick Innovation Foundation Research Assistant's Initiative and Graduate Scholarships programs. The authors also thank Yang Zhan, Rongrong Gu, Zizhen Gao and Luji Xiong for their volunteer work to collect field data in the Urban Site.

REFERENCES

- Aghayari, S., Saadatseresht, M., Omidalizarandi, M., Neumann, I., 2017. Geometric Calibration of Full Spherical Panoramic Ricoh-Theta Camera. *ISPRS Annals of Photogrammetry, Remote Sensing and Spatial Information Sciences IV-1/W1*, 237–245. at: <https://doi.org/10.5194/isprs-annals-IV-1-W1-237-2017>
- Bell, J.F., Iles, K., Marshall, D., 1983. Balancing the ratio of tree count-only sample points and VBAR measurements in variable plot sampling., in: Bell J.F. and Atterbury, T. (Eds.). *Proceedings: Renewable Resource Inventories for Monitoring Changes and Trends*. College of Forestry, Oregon State University, Corvallis, OR, pp. 699–702.
- Belton, D., Moncrieff, S., Chapman, J., 2013. Processing tree point clouds using Gaussian Mixture Models, in: *ISPRS Annals of Photogrammetry, Remote Sensing and Spatial Information Sciences*. Presented at the ISPRS Workshop Laser Scanning 2013, Copernicus GmbH, Antalya, Turkey, pp. 43–48. at: <https://doi.org/10.5194/isprsannals-II-5-W2-43-2013>
- Berveglieri, A., Tommaselli, A., Liang, X., Honkavaara, E., 2017. Photogrammetric measurement of tree stems from vertical fisheye images. *Scandinavian Journal of Forest Research* 32, 737–747. at: <https://doi.org/10.1080/02827581.2016.1273381>
- Bitterlich, W., 1984. *The relascope idea: Relative measurements in forestry*, First. ed. CAB International, Slough, England.
- Blake, J., Somers, G., Ruark, G., 1991. Estimating limiting foliar biomass in conifer plantations from allometric relationships and self-thinning behavior. *For Sci* 37, 296–307.
- Celes, C.H.S., Araujo, R.F. de, Emmert, F., Lima, A.J.N., Campos, M.A.A., Celes, C.H.S., Araujo, R.F. de, Emmert, F., Lima, A.J.N., Campos, M.A.A., 2019. Digital Approach for Measuring Tree Diameters in the Amazon Forest. *Floresta e Ambiente* 26. at: <https://doi.org/10.1590/2179-8087.038416>
- Clark, N., Wynne, R.H., Schmoldt, D.L., Araman, P.A., Winn, M.F., 1998. Use of a non-metric digital camera for tree stem evaluation, in: *Proceedings, 1998 ASPRS/RT Annual Convention*. (Pre-Published Version).
- Clark, N.A., Wynne, R.H., Schmoldt, D.L., 2000a. A review of past research on dendrometers. *For Sci* 46, 570–576.
- Clark, N.A., Wynne, R.H., Schmoldt, D.L., Winn, M., 2000b. An assessment of the utility of a non-metric digital camera for measuring standing trees. *Computers and Electronics in Agriculture* 28, 151–169. at: [https://doi.org/10.1016/S0168-1699\(00\)00125-3](https://doi.org/10.1016/S0168-1699(00)00125-3)
- Dai, X., 2018. Bias correction in panoramic photo-based angle count sampling. Unpub. BScF Honors. University of New Brunswick, Fredericton, NB, Canada.
- Dai, X., Ducey, M.J., Kershaw, J.A., Jr., Wang H., In review. Sector subsampling as an alternative to big-BAF sampling. *Canadian Journal of Forest Research*.
- Dean, C., 2003. Calculation of wood volume and stem taper using terrestrial single-image close-range photogrammetry and contemporary software tools. *Silva Fenn.* 37, 359–380.
- DeCourt, N., 1956. Utilisation de la photographie pour mesurer les surfaces terrières (The use of photography for measuring basal area). *Rev For Fran* 8, 505–507.
- Dick, A.R., 2012. Forest inventory using a camera: Concept, field implementation and instrument development (Unpublished MScF Thesis). University of New Brunswick, Fredericton, NB, Canada.
- Dick, A.R., Kershaw, J.A., MacLean, D.A., 2010. Spatial Tree Mapping Using Photography. *north j appl for* 27, 68–74. at: <https://doi.org/10.1093/njaf/27.2.68>
- Donnelly J.G., Lavigne M.B., van Nostrand D.A., 1986. Precommercial Thinning Spacing Trials Established Between 1979 and 1985. Newfoundland Forestry Centre, St. John's Newfoundland, Canada.

- Fang, R., and B. Strimbu. 2017. Photogrammetric point cloud trees. *Mathematical and Computational Forestry & Natural Resource Sciences* 9:30–33. at: <http://www.mcfns.net/index.php/Journal/article/view/9.8>.
- Fastie, C.L., 2010. Estimating stand basal area from forest panoramas, in: *Proceedings of the Fine International Conference on Gigapixel Imaging for Science*. Carnegie Mellon University, Pittsburg, PA, p. 8.
- Forsman, M., Börlin, N., Holmgren, J., 2016. Estimation of Tree Stem Attributes Using Terrestrial Photogrammetry with a Camera Rig. *Forests* 7, 61. at: <https://doi.org/10.3390/f7030061>
- Gadow, K. von, Zhang, C.Y., Zhao, X.H., 2009. Science-based Forest Design. *Mathematical and Computational Forestry & Natural-Resource Sciences (MCFNS)* 1, 14-25 (12). at: <http://mcfns.net/index.php/Journal/article/view/MCFNS.1-14>
- Gollob, C., Ritter, T., Wassermann, C., Nothdurft, A., 2019. Influence of Scanner Position and Plot Size on the Accuracy of Tree Detection and Diameter Estimation Using Terrestrial Laser Scanning on Forest Inventory Plots. *Remote Sensing*, 11(13), 1602. at: <https://doi.org/10.3390/rs11131602>.
- Grosenbaugh, L.R., 1963. Optical dendrometers for out-of-reach diameters: A conspectus and some new theory. *For Sci Monog* 4, 48. at: <https://doi.org/10.1093/forestscience/9.s2.a0001>
- Guido, van R., 2018. Python (programming language). Python Software Foundation, US.
- Hayashi, R., Kershaw, J.A., Jr., Weiskittel, A.R., 2015. Evaluation of alternative methods for using LiDAR to predict aboveground biomass in mixed species and structurally complex forests in north-eastern North America. *Mathematical and Computational Forestry & Natural Resources Sciences* 7, 49–65. at: http://mcfns.net/index.php/Journal/article/view/MCFNS7.2_2
- Hodges, J.L., 1958. The significance probability of the smirnov two-sample test. *Ark. Mat.* 3, 469–486. at: <https://doi.org/10.1007/BF02589501>
- Husch, B., 1980. How to determine what you can afford to spend on inventories, in: *IUFRO Workshop on Arid Land Resource Inventories*. USDA, Forest Service, Washington Office, General Technical Report WO-28, La Paz, Mexico, pp. 98–102.
- Iles, K., 2003. *A sampler of inventory topics*, 2nd ed. Kim Iles and Associates, Nanaimo, BC.
- Iles, K., 2012. Some Current Subsampling Techniques in Forestry. *Mathematical and Computational Forestry & Natural-Resource Sciences* 4, 77–80. at: http://mcfns.net/index.php/Journal/article/view/143/MCFNS-4.2_77
- Kershaw, J.A., Jr., Ducey, M.J., Beers, T.W., Husch, B., 2016. *Forest Mensuration*, 5th ed. Wiley/Blackwell, Hoboken, NJ.
- Lambert, M.C., Ung, C.H., Raulier, F., 2005. Canadian national tree aboveground biomass equations. *Can J For Res* 35, 1996–2018. at: <https://doi.org/10.1139/x05-112>
- Larsen, D.R., 2006a. Use of very high resolution digital oblique photography in the development of 3-dimensional models for tree measurements: Examples from ground based and aerial based platforms. Presented at the Proceedings of the 20th Biennial Workshop on Color Photography, Videography and Airborne Imaging for Resource Assessment., American Society of Photogrammetry and Remote Sensing (published by ASPRS on CD).
- Larsen, D.R., 2006b. Development of a photogrammetric method of measuring tree taper outside bark. *Gen. Tech. Rep. SRS-92*. Asheville, NC: U.S. Department of Agriculture, Forest Service, Southern Research Station. pp. 347-350.
- Liang, X., Jaakkola, A., Wang, Y., Hyyppä, J., Honkavaara, E., Liu, J., Kaartinen, H., 2014. The Use of a Hand-Held Camera for Individual Tree 3D Mapping in Forest Sample Plots. *Remote Sensing* 6, 6587–6603. at: <https://doi.org/10.3390/rs6076587>
- Liang, X., Wang, Y., Jaakkola, A., Kukko, A., Kaartinen, H., Hyyppä, J., Honkavaara, E., Liu, J., 2015. Forest Data Collection Using Terrestrial Image-Based Point Clouds From a Handheld Camera Compared to Terrestrial and Personal Laser Scanning. *IEEE Transactions on Geoscience and Remote Sensing* 53, 5117–5132. at: <https://doi.org/10.1109/TGRS.2015.2417316>
- Liu, J., Feng, Z., Yang, L., Mannan, A., Khan, T.U., Zhao, Z., Cheng, Z., 2018. Extraction of Sample Plot Parameters from 3D Point Cloud Reconstruction Based on Combined RTK and CCD Continuous Photography. *Remote Sensing* 10, 1299. at: <https://doi.org/10.3390/rs10081299>
- Lu, M.K., Lam, T.Y., Perng, B.-H., Lin, H.-T., 2019. Close-range photogrammetry with spherical panoramas for mapping spatial location and measuring diameters of trees under forest canopies. *Can. J. For.*

- Res. 49, 865–874. at: <https://doi.org/10.1139/cjfr-2018-0430>
- Marshall, D.D., Iles, K., Bell, J.F., 2004. Using a large-angle gauge to select trees for measurement in variable plot sampling. *Can J For Res* 34, 840–845. at: <https://doi.org/10.1139/x03-240>
- Miller, J., Morgenroth, J., Gomez, C., 2015. 3D modelling of individual trees using a handheld camera: Accuracy of height, diameter and volume estimates. *Urban Forestry & Urban Greening* 14, 932–940. at: <https://doi.org/10.1016/j.ufug.2015.09.001>
- Mokroš, M., Výboštok, J., Tomašík, J., Grznárová, A., Valent, P., Slavík, M., Merganič, J., 2018. High Precision Individual Tree Diameter and Perimeter Estimation from Close-Range Photogrammetry. *Forests* 9, 696. at: <https://doi.org/10.3390/f9110696>
- Mulverhill, C., Coops, N.C., Tompalski, P., Bater, C.W., Dick, A.R., 2019. The utility of terrestrial photogrammetry for assessment of tree volume and taper in boreal mixedwood forests. *Annals of Forest Science* 76, 83. at: <https://doi.org/10.1007/s13595-019-0852-9>
- Pan, Y., Birdsey, R.A., Phillips, O.L., Jackson, R.B., 2013. The Structure, Distribution, and Biomass of the World's Forests. *Annual Review of Ecology, Evolution, and Systematics* 44, 593–622. at: <https://doi.org/10.1146/annurev-ecolsys-110512-135914>
- Pengle, C., Jinhao, L., Dian, W., 2013. Measuring diameters at breast height using combination method of laser and machine vision (In Chinese). *Transactions of the Chinese Society for Agricultural Machinery* 44, 271–275.
- Perng, B.H., Lam, T.Y., Lu, M.K., 2018. Stereoscopic imaging with spherical panoramas for measuring tree distance and diameter under forest canopies. *Forestry (Lond)* 91, 662–673. at: <https://doi.org/10.1093/forestry/cpy028>
- Reineke, L.H., 1940. Permanent sample plot photography. *Journal of Forestry* 38, 813–815.
- Reu, P. L., Sweatt, W., Miller, T., Fleming, D., 2014. Camera system resolution and its influence on digital image correlation (Report No. SAND2013-8737J; p. 26). Albuquerque, NM: Sandia National Laboratory.
- Ricoh Imaging Company, LTD., 2016. Ricoh Theta S 360 video camera [WWW Document]. THETA S — RICOH IMAGING. at: http://www.ricoh-imaging.co.jp/english/products/theta_s.
- Ritter, T., Nothdurft, A., Saborowski, J., 2013. Correcting the nondetection bias of angle count sampling. *Canadian Journal of Forest Research*. 43, 344–354. at: <https://doi.org/10.1139/cjfr-2012-0408>.
- Ringdahl, O., Hohnloser, P., Hellström, T., Holmgren, J., Lindroos, O., 2013. Enhanced Algorithms for Estimating Tree Trunk Diameter Using 2D Laser Scanner. *Remote Sensing* 5, 4839–4856. at: <https://doi.org/10.3390/rs5104839>
- Rodríguez-García, C., Montes, F., Ruiz, F., Cañellas, I., Pita, P., 2014. Stem mapping and estimating standing volume from stereoscopic hemispherical images. *Eur J Forest Res* 133, 895–904. ar: <https://doi.org/10.1007/s10342-014-0806-6>
- Sánchez-González, M., Cabrera, M., Herrera, P.J., Vallejo, R., Cañellas, I., Montes, F., 2016. Basal Area and Diameter Distribution Estimation Using Stereoscopic Hemispherical Images. *Photogrammetric Engineering & Remote Sensing* 82, 605–616. at: <https://doi.org/10.14358/PERS.82.8.605>
- Shimizu, A., Yamada, S., Arita, Y., 2014. Diameter Measurements of the Upper Parts of Trees Using an Ultra-Telephoto Digital Photography System. *Open Journal of Forestry* 4, 316–326. at: <https://doi.org/10.4236/ojf.2014.44038>
- Smith, W.B., Brand, G.J., 1983. Allometric biomass equations for 98 species of herbs, shrubs, and small trees (Research Note No. RN-NC-299). USDA, Forest Service, North Central Forest Experiment Station.
- Snavely, N., Seitz, S.M., Szeliski, R., 2008. Modeling the World from Internet Photo Collections. *International Journal of Computer Vision* 80, 189–210. at: <https://doi.org/10.1007/s11263-007-0107-3>
- Stewart, B., 2004. Using a camera as an angle gauge in angle-count sampling (MF Thesis). The University of Georgia.
- Surový, P., Yoshimoto, A., Panagiotidis, D., 2016. Accuracy of Reconstruction of the Tree Stem Surface Using Terrestrial Close-Range Photogrammetry. *Remote Sensing* 8, 123. at: <https://doi.org/10.3390/rs8020123>
- Varjo, J., Henttonen, H., Lappi, J., Heikkonen, J., Juujärvi, J., 2006. Digital horizontal tree measurements for forest inventory. Working papers of the Finnish Forest Research Institute 23.
- Wang, H., 2017. Extracting DBH measurements from RGB photo images. Unpub. BScF Honors. The

- University of New Brunswick, Fredericton, NB, Canada. at: <http://rgdoi.net/10.13140/RG.2.2.30588.77440>
- Wang, H., 2019. Estimating Forest Attributes from Spherical Images. MSc Forestry thesis. The University of New Brunswick, Fredericton, NB, Canada. at: <https://www.doi.org/10.13140/RG.2.2.35680.64004>
- Wang, H., Kershaw, J.A., Yang, T.R., Hsu, Y.H., Ma, X., Chen, Y., 2020. An Integrated System for Estimating Forest Basal Area from Spherical Images. *Mathematical and Computational Forestry & Natural-Resource Sciences*. at: <http://mcfns.net/index.php/Journal/article/view/12.1>
- Xing, Z., Bourque, C.P.A., Swift, D.E., Clowater, C.W., Krasowski, M., Meng, F.R., 2005. Carbon and biomass partitioning in balsam fir (*Abies balsamea*). *Tree Physiol* 25, 1207–1217.
- Yang, T.R., Hsu, Y.H., Kershaw, J.A., McGarrigle, E., Kilham, D., 2017. Big BAF sampling in mixed species forest structures of northeastern North America: influence of count and measure BAF under cost constraints. *Forestry (Lond)* 90, 649–660. at: <https://doi.org/10.1093/forestry/cpx020>
- Zar, J.H., 2009. *Biostatistical analysis*, 5th ed. Pearson, New York.
- Zianis, D., Muukkonen, P., Mäkipää, R., Mencuccini, M., 2005. Biomass and stem volume equations for tree species in Europe. *Silva Fenn Monog* 4, 63.